Neutral Sulfuric Acid-Water Clustering Rates: Bridging the Gap between Molecular Simulation and Experiment

Philip T. M. Carlsson,[*,†,§] Steven Celik,[†] Daniel Becker,[†] Tinja Olenius,[‡,∥] Jonas Elm,[¶] and Thomas Zeuch[†]

†*Institut für Physikalische Chemie, Universität Göttingen, 37077 Göttingen, Germany*

‡*Department of Environmental Science and Analytical Chemistry & Bolin Centre for Climate Research, Stockholm University, 10691 Stockholm, Sweden*

¶*Department of Chemistry and iClimate, Aarhus University, 8000 Aarhus C, Denmark*

§*now at IEK-8, Forschungszentrum Jülich GmbH, 52425 Jülich, Germany*

∥*now at Swedish Meteorological and Hydrological Institute, 60176 Norrköping, Sweden*

E-mail: p.carlsson@fz-juelich.de

Keywords: Nucleation, Sulfuric Acid, Kinetics, Atmospheric Chemistry, Aerosols

Abstract

The role of sulfuric acid during atmospheric new particle formation is an ongoing topic of discussion. In this work, we provide quantitative experimental constraints for quantum chemically calculated evaporation rates for the smallest H_2SO_4−H_2O clusters, characterising the mechanism governing nucleation on a kinetic, single molecule level. We compare experimental particle size distributions resulting from a highly supersaturated homogeneous H_2SO_4 gas phase with the results from kinetic simulations employing quantum chemically derived decomposition rates of electrically neutral H_2SO_4 molecular clusters up to the pentamer at large range of relative humidities. By using high H_2SO_4 concentrations, we circumvent the uncertainties concerning contaminants and competing reactions present in studies at atmospheric conditions. We show good agreement between molecular simulation and experimental measurements and provide the first evaluation of theoretical predictions of the stabilisation provided by water molecules.

Graphical TOC Entry

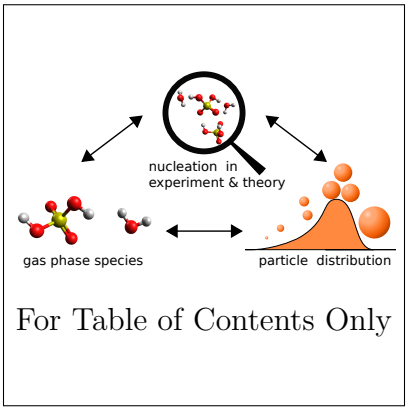

For Table of Contents Only

New particle formation in the atmosphere is known to have a large effect on earth's climate and is often connected to the availability of sulfuric acid (H_2SO_4).[1,2] H_2SO_4 forms molecular clusters with water and further stabilising species such as amines[3,4] or organic acids[5–7] that can then grow large enough to act as cloud condensation nuclei. Measurements at the CLOUD chamber, CERN, have provided experimental data from which cluster thermochemistry data was recently extracted for the sulfuric acid-ammonia system.[8,9] For small neutral clusters, the usually employed mass spectrometric techniques are challenging to apply since they require an initial charging of the clusters, which is expected to affect the molecular composition.[10–13] However, neutral nucleation may dominate over ion-mediated nucleation in many environments.[14] Even key parameters of neutral nucleation remain under discussion, for instance the collision rate between H_2SO_4 clusters where long range forces enhance the rate of clustering.[15]

In previous work, we have shown an experiment where a homogeneously supersaturated gas phase of H_2SO_4 is formed during ozonolysis of 2-butene in the presence of SO_2 *via* its rapid oxidation by stabilized Criegee intermediates (sCI).[16] This provides a new pathway that is able to yield higher supersaturation than in previous experiments with temporal control *via* known reaction kinetics.[17,18] The *in situ* formation of H_2SO_4 removes the otherwise prevalent influence of the concentration inhomogeneities at an inlet nozzle while wall losses at least in the initial phase of nucleation are diminished by the high concentrations. Since the discovery of this system, we have developed a kinetic model from first principles where the evolving particle size distribution (PSD) can be calculated from the gas phase.[19] There we were able to show a high sensitivity of the resulting PSD towards the used clustering rates. Now we use this sensitivity to evaluate quantum chemically derived aggregation kinetics and thereby investigate the underlying cluster energetics for the stabilising effect of water molecules on sulfuric acid clusters.

The experimental set-up and procedures have been discussed in detail in previous works, therefore only the main features are described below.[20–23] The ozonolysis experiments were

conducted at ∼450 mbar in a static reactor with a volume of 64 L. For all relevant reactions, we expect this to be at least close to the high pressure limit.[21] For better comparability with the bulk of experiments at tropospheric pressure, all concentrations below are given in terms of mole fractions against 1 bar reference pressure, noting that the real mole fractions are a factor of ∼2.2 larger. Reactant concentrations were determined volumetrically for all substances except ozone, where UV absorption was employed. A calibrated dilution of SO_2 in N_2 was used to achieve the SO_2 concentrations. Reactant and product concentrations in the reactor were determined using Fourier Transform Infrared Spectroscopy (Bruker Vertex 70v FTIR spectrometer, 12 m path length in the reactor through use of a multipass White cell), where applicable. All chemicals used were of commercial grade (see supporting information). The reactive mixture was prepared by rapidly (within ∼2 s) expanding a mixture of 2-butene (mixture of *cis* and *trans*) with synthetic air as well as ozone with synthetic air from two premixing chambers, both with a volume of 40.5 L, into the reactor, resulting in 18 ppm 2-butene and 0.85 ppm ozone. The temperature during the expansion increases to 305 K before homogenising and decreasing to 298 K within a few seconds. During the experiment, it slowly further decreases to reach 295.5±0.5 K dictated by a thermostat cooling the inner shell of the double-shell construction. SO_2 and water were added directly to the reactor ahead of the expansion. Ozonolysis reaction time was 300 s in all experiments. After this time, the ozone was completely consumed and the particle size distribution only changed slowly and marginally with wall losses, dilution, and coagulation. The rates for these processes have been determined in earlier work.[19] To perform the particle analysis, synthetic air was added to the reaction cell up to a pressure of 1 bar. The particle size distributions were measured with a particle classifier (TSI SMPS 3938EL57 with LDMA 3081A and NDMA 3085A as well as TSI CPC 3750, operation parameters: 2 litres per minute (lpm) sheath flow and 0.2 lpm sample flow). A series of 6 particle size distributions was measured for each experiment, where the first scan time was used to equalize the in- and outflow rates and therefore disregarded in the analysis. The particle number concentrations

have been calculated from the obtained values of $\mathrm{d}N/\mathrm{d}\log(d_p)$ for ease of comparison with the simulations.. Fig. 1 shows the influence of the addition of water on the resulting particle size distribution.

The main aspects of the particle dynamics model have been presented in a previous publication.[19] Since these previous reference experiments were only performed at dry conditions, the reactions of the water monomer and dimer with the sCI were added to account for their influence at the higher water contents present (see reaction mechanism in the supplementary data). Beyond that, the gas phase kinetics calculations use the reaction mechanism developed in earlier work[16] and were calculated with the Logesoft 1.02.013 software package.[25] For the particle phase (i.e. where the cluster reactions are no longer treated molecule-by-molecule, starting at the hexamer), the temporal development of the whole ensemble of particles due to coagulation, condensation, evaporation, wall losses, and dilution is modelled as a set of kinetic equations without explicit treatment of the cluster energetics. We adapt the sectional model as described by Gelbard and Seinfeld,[26] since it allows for a very flexible description regardless of the number of components in the system or the modality of the distribution. We chose to increase the section size with increasing particle size in a manner that keeps the position and size of the sections in agreement with our experimental equipment, following expression (1):

$$d_i = d_\alpha \times \left(\frac{d_\Omega}{d_\alpha}\right)^{\frac{i-1}{i_{tot}-1}} . \tag{1}$$

Here d_i is the lower boundary of section number i, d_α that of the smallest section, d_Ω that of the largest section and i_{tot} the total number of sections. Usually, the section size follows $d_{i+1} = d_i \times f_s$ with f_s as a constant factor. If f_s is lower than 1.08, the discrepancies towards non-sectional methods become almost negligible.[27] For our sections, the corresponding value for f_s would be smaller at around 1.0365. By implementing a moving average size of the particles in the respective bins, we circumvent the problem of numerical diffusion.[27,28]

The kernels governing the condensation and coagulation have been left unchanged since the last publication, where they were validated against the temporal evolution of the experimental size distribution.[19] The crucial set of non-determined parameters in the simulation are the decomposition rates of the initial H_2SO_4−H_2O molecular clusters containing up to five H_2SO_4 molecules. In the previous publication,[19] they were arbitrarily chosen purely to determine the sensitivity of the resulting size distribution on the initial nucleation rates. Now we calculate the rates from the Gibbs free energies of formation of the clusters instead, obtained from quantum chemistry.[29] Different from the treatment by Kürten,[9] the influence of water is calculated explicitly for these clusters. Each cluster with a given number of H_2SO_4 molecules was assumed to be hydrated by up to five H_2O molecules. As the rate coefficients of water condensation and evaporation are orders of magnitude higher than those of H_2SO_4, the clusters are assumed to be in equilibrium with respect to water and the decomposition rates are calculated as effective values over the hydrate distributions. The decomposition rate of cluster $i+j$ into clusters i and j is

$$\gamma_{i+j\rightarrow i,j} = \beta_{i,j}\frac{P_{\mathrm{ref}}}{k_{\mathrm{B}}T}\exp\left(\frac{\Delta G_{i+j}-\Delta G_i-\Delta G_j}{k_{\mathrm{B}}T}\right), \tag{2}$$

where ΔG_i is the formation free energy of cluster i with respect to monomers, calculated at reference pressure P_{ref}, T is the temperature, and k_{B} is the Boltzmann constant. $\beta_{i,j}$ is the rate coefficient of the corresponding molecular collision, calculated here as the hard-sphere collision rate. This neglects additional attractive potentials and will therefore be a lower limit to the true value, but since changing the collision rates also changes the evaporation rates to have the opposite effect, this does not significantly impede the model comparisons in this work. Eq. (2) is calculated for all hydrates of cluster $i+j$ decomposing into hydrates of clusters i and j, and the effective rate is obtained as

$$\gamma^{\mathrm{eff}}_{i+j\rightarrow i,j} = \sum_{n=0}^{n_{\max}}\sum_{m=0}^{n_{\max}-n}\gamma_{i+j,n+m\rightarrow i,n;j,m}f_{i+j,n+m}. \tag{3}$$

In Eq. (3), n and m are the numbers of H_2O molecules in the decomposition products i and j, $n_{\max} = 5$ is the maximum number of water molecules in the clusters, and $f_{i+j,n+m}$ is the fraction of hydrates containing $n + m$ water molecules in the hydrate distribution of cluster $i + j$. The hydrate distributions are calculated from the free energies of hydration as described in Henschel *et al.*[30]

Two different quantum chemically derived data sets were used to assess the decomposition rate coefficients: previously published data calculated at the RICC2/aug-cc-pV(T+d)Z//B3LYP/CBSB7 level of theory,[30] and updated data obtained applying the recently developed DLPNO method[31,32] at the DLPNO-CCSD(T)/aug-cc-pVTZ//ωB97X-D/6-31++G(d,p) level. It should be noted that the DLPNO calculations are based on re-optimization of the original lowest free energy B3LYP/CBSB7 structures and that no new configurational sampling has been applied (data can be found in the Atmospheric Cluster Database[33]). Generally, the previously used RICC2 method tends to overpredict cluster binding and yield more random errors, while the DLPNO method tends to underpredict it while giving more robust results.[34,35] The rates resulting from the quantum chemical calculations were further multiplied with a scaling factor to bring the simulated size distributions to the best possible agreement with the experiments, given in tab. 1 and shown in fig. 4. As illustrated in fig. 2 as well as the previous publication,[19] the sensitivity towards the decomposition rates enables us to pinpoint overall rates of nucleation within a factor of 2.

A comparison of the final decomposition rates shows two striking differences in the water dependency (see tab. 1). Firstly, the RICC2 method predicts a drastic stabilisation of the trimer already at 5 mbar of added water, while DLPNO only gives a moderate influence. Since the wet rates are calculated as weighted sums over all the possible decomposition paths of a respective cluster, the dependence of the effective rate on the stabilities of individual hydrates is highly non-linear. Secondly and probably connected to this effect, RICC2 shows the decomposition to a trimer and a monomer as the most likely reaction of a hydrated tetramer. In contrast, for DLPNO the ratio between the trimer and monomer decompo-

Table 1: Calculated effective decomposition rates (in s^{-1}) of H_2SO_4−H_2O molecular clusters at varying water partial pressures along with their scaling factor that best brings the simulation in agreement with the experiment for 100 ppb initial SO_2 for the RICC2 (top) and DLPNO (bottom) method. Rates for the pentamers were taken from the dry values for 10 ppm H_2O and interpolated between the tetramer decomposition rates and the evaporation rates from particles for the wet cases (see supplementary data), since no hydrated calculated rates were available. A=H_2SO_4

Method	Reaction	10 ppm	5 mbar	10 mbar	15 mbar	20 mbar
	$A_2 \longrightarrow 2\,A$	$5.15{\cdot}10^3$	$2.42{\cdot}10^3$	$1.45{\cdot}10^3$	$1.00{\cdot}10^3$	$7.61{\cdot}10^2$
	$A_3 \longrightarrow A_2 + A$	$1.37{\cdot}10^5$	$6.21{\cdot}10^2$	$2.35{\cdot}10^2$	$1.71{\cdot}10^2$	$1.52{\cdot}10^2$
	$A_4 \longrightarrow A_3 + A$	$4.66{\cdot}10^3$	$2.91{\cdot}10^3$	$6.49{\cdot}10^3$	$1.15{\cdot}10^4$	$1.79{\cdot}10^4$
RICC2	$A_4 \longrightarrow A_2 + A_2$	$2.58{\cdot}10^4$	$1.5{\cdot}10^2$	$1.9{\cdot}10^2$	$3{\cdot}10^2$	$4{\cdot}10^2$
	$A_5 \longrightarrow A_4 + A$	$4.91{\cdot}10^4$	$2.11{\cdot}10^3$	$4.60{\cdot}10^3$	$8.14{\cdot}10^3$	$1.27{\cdot}10^4$
	$A_5 \longrightarrow A_3 + A_2$	$1.63{\cdot}10^4$	–	–	–	–
Best fit scaling factor, 100 ppb SO_2		**3**	**8.5**	**7.5**	**6.25**	**5**
Best fit scaling factor, 10 ppb SO_2		**0.525**	**0.90**	**0.70**	**0.60**	**0.50**
	$A_2 \longrightarrow 2\,A$	$1.48{\cdot}10^5$	$1.46{\cdot}10^5$	$1.35{\cdot}10^5$	$1.22{\cdot}10^5$	$1.11{\cdot}10^5$
	$A_3 \longrightarrow A_2 + A$	$4.90{\cdot}10^6$	$4.85{\cdot}10^6$	$3.79{\cdot}10^6$	$2.44{\cdot}10^6$	$1.58{\cdot}10^6$
	$A_4 \longrightarrow A_3 + A$	$2.90{\cdot}10^4$	$3.30{\cdot}10^4$	$5.13{\cdot}10^4$	$9.34{\cdot}10^4$	$1.60{\cdot}10^5$
DLPNO	$A_4 \longrightarrow A_2 + A_2$	$1.99{\cdot}10^5$	$2.27{\cdot}10^5$	$2.92{\cdot}10^5$	$3.74{\cdot}10^5$	$4.60{\cdot}10^5$
	$A_5 \longrightarrow A_4 + A$	$1.78{\cdot}10^4$	$1.79{\cdot}10^5$	$2.37{\cdot}10^5$	$3.22{\cdot}10^5$	$3.22{\cdot}10^5$
	$A_5 \longrightarrow A_3 + A_2$	$1.27{\cdot}10^3$	–	–	–	–
Best fit scaling factor, 100 ppb SO_2		**0.25**	**0.065**	**0.0285**	**0.016**	**0.01**
Best fit scaling factor, 10 ppb SO_2		**0.04**	**0.006**	**0.0028**	**0.0015**	**0.001**

sition and the dimer and dimer decomposition remains similar to the dry case. However, changing the decomposition pathway even from pure dimer formation to pure trimer and monomer formation has no significant impact on the resulting particle size distribution from the simulation as long as the overall decomposition rate of the tetramer remains constant.

From the evaporation rates of H_2SO_4 from the largest clusters, an approximation of macroscopic saturation pressures can be made (shown in tab. 2, see SI for details). Here further discrepancies between the methods become apparent: for increasing humidity, the saturation pressures derived from DLPNO decrease and even show qualitative agreement with macroscopic experimental data (see fig.1 in the SI)[36] while the values derived from the RICC2 calculations show unphysical behaviour with an increase of saturation pressures. It should be noted that allowing the evaporation from clusters with more than five H_2SO_4

Table 2: Variation of the effective saturation pressures ($c_{eff} = c_{sat} \cdot X_m \cdot \gamma_m$) of H_2SO_4 to give a consistent description of the evaporation from clusters and particles for the respective sets of decomposition rates (see table 1).

Water	RICC2		DLPNO	
content	p_{eff}/ Pa	c_{eff}/ 1/m^3	p_{eff}/ Pa	c_{eff}/ 1/m^3
10 ppm	$1.9{\cdot}10^{-6}$	$4.8{\cdot}10^{14}$	$8.0{\cdot}10^{-6}$	$2.0{\cdot}10^{15}$
5 mbar	$3.6{\cdot}10^{-6}$	$8.8{\cdot}10^{14}$	$2.3{\cdot}10^{-6}$	$5.7{\cdot}10^{14}$
10 mbar	$6.9{\cdot}10^{-6}$	$1.7{\cdot}10^{15}$	$1.4{\cdot}10^{-6}$	$3.3{\cdot}10^{14}$
15 mbar	$1.0{\cdot}10^{-5}$	$2.5{\cdot}10^{15}$	$1.0{\cdot}10^{-6}$	$2.5{\cdot}10^{14}$
20 mbar	$1.3{\cdot}10^{-5}$	$3.1{\cdot}10^{15}$	$8.6{\cdot}10^{-7}$	$2.1{\cdot}10^{14}$

molecules only insignificantly changes the resulting particle size distribution under these conditions since the impact of the loss of singular H_2SO_4 molecules becomes smaller with increasing particle size.

With the tools now at our disposal, we are able to differentiate between three regimes of particle dynamics. For higher SO_2 concentrations (starting above 200 ppb initial SO_2), as can be seen in fig. 3, additional mass is necessary to bring the simulated size distribution in agreement with the experiment regardless of the scaling factors used for the nucleation reaction. Since this necessity is only seen for particle size distributions with comparatively long residence times and large mean sizes, a source could be reactive uptake of small oxidised organic molecules from the 2-butene ozonolysis; however any further analysis would be pure speculation so the results from these higher concentrations are disregarded for now.

A second regime is identified at low initial concentrations (10 ppb SO_2 and below), where the necessary multiplicators are below unity even for the RICC2 values (see the filled and open squares in fig. 4). This is counterintuitive with regards to the general overprediction of the cluster stability with this method,[34] we therefore conclude that for these low concentrations, additional stabilising species such as oxidation products from the 2-butene ozonolysis or amines introduced as impurities may start to play a role in the nucleation mechanism. This is in agreement with the influence of impurities seen in atmospheric chamber experiments.

In a third regime with initial SO_2 values around 100 ppb (corresponding to ∼20 ppb peak H_2SO_4 concentration), both the RICC2 and DLPNO scaling factors are in agreement with

their respective oppositional biases (see filled and open triangles in fig. 4). For the dry decomposition rates only a scaling factor of 3 and 0.5 for RICC2 and DLPNO, respectively, is necessary to bring the simulations in agreement with the experiment. The errors are expected to be the smallest in the dry case since the dry clusters have significantly fewer degrees of freedom, lowering the complexity. These factors correspond to modifying the reaction free energies (Eq. 2) by less than 1 kcal/mol, which is well within the typical uncertainty of quantum chemical methods. Both methods are therefore able to reproduce the dry nucleation rate well. At increasing water content, the two methods start to diverge. While the RICC2 values show the overall smaller dependency of the scaling factor on water content, the DLPNO factors have to be monotonously decreased. As stated by Myllys *et al.*,[34] this might be related to a systematic underestimation of the binding energies by the DLPNO method, which becomes more pronounced for larger clusters. Since species such as highly hydrated H_2SO_4 clusters are promoted by higher relative humidities, their systematically underpredicted stabilities gain more influence in equation 3. On the other hand, RICC2 may benefit from error compensation: while it tends to overpredict cluster stability, the structural sampling may have the opposite effect if the most stable cluster structures are not found, giving reduced net errors. This can also be a consequence of the lack of new configurational sampling. The incorrect humidity influence on the saturation pressure for RICC2 indicates such masked errors (see tab. 2 and fig. 1 in the SI). Varying the reaction rate of water and its dimer with the sCI also changes the resulting total particle mass (compare fig. 1), but no influence on the necessary scaling factors was found.

To summarise, we show how rapid oxidation of SO_2 through stabilized Criegee intermediates produces a highly supersaturated H_2SO_4 gas phase at different degrees of humidity. Under certain experimental conditions, homogeneous nucleation of H_2SO_4 is the dominating if not the only relevant nucleation reaction. Comparing experimental particle size distributions with the results from kinetic simulations employing quantum chemically derived decomposition rates of the neutral H_2SO_4 clusters gives direct insight into the molecular

nucleation mechanism while also providing the correct sinks to prevent overestimation of new particle formation. This approach allows us to reduce the complexity of the particle formation problem, as nucleation becomes the key process for the evolution of the particle size distribution. We are able to show the good agreement – within the correct order of magnitude – of the quantum chemically derived cluster decomposition rates with rates necessary to correctly describe the experimental particle size distributions. We also provide the first evaluation of the stabilisation provided by water molecules, where the DLPNO derived stabilisation is too small and therefore the decomposition rates are overestimated over the whole range of cluster sizes. Still, the values for the tetramer generate saturation pressures in qualitative agreement with experimental values. The RICC2 values provide a better fit to the experimental particle data, however possibly affected by beneficial error compensation due to incomplete sampling of the formed hydrate clusters as the corresponding saturation pressures show. Since water has a large influence on cluster formation and the resulting particle size distribution, further configurational sampling of hydrated cluster systems using systematic hydrated sampling techniques is clearly needed to further improve the calculated nucleation rates.[37,38] Additionally, an extension of the investigated cluster sizes beyond the tetra- and pentamer, possibly also with experimental studies,[39] would help to lessen the uncertainty introduced by specific cluster structures.

By resolving the sulfuric acid and sulfuric acid - water nucleation mechanism and bridging the gap between molecular simulation and experiment to investigate the nucleation rates, we are taking one step further towards calculating the concentration of newly formed cloud condensation nuclei directly from the atmospheric gas phase composition.

Acknowledgments

This work is supported by the German Research Foundation (grants ZE 890 3-1 and ZE 890 3-2, project number 250936489). T. O. thanks the ÅForsk Foundation (project 18-334) and

the K.&A. Wallenberg Foundation (Academy Fellowship AtmoRemove); D. B. the Verband der Chemischen Industrie (grant 104371) for financial support. The continuous support of Prof. Dr. Martin Suhm is gratefully acknowledged.

Associated Content

List of used chemicals, coagulation and condensation kernels, details on the used gas phase mechanism; supplementary results concerning the evaporation rates from larger particles

References

(1) Kulmala, M.; Riipinen, I.; Sipilä, M.; Manninen, H. E.; Petäjä, T.; Junninen, H.; Maso, M. D.; Mordas, G.; Mirme, A.; Vana, M. et al. Toward Direct Measurement of Atmospheric Nucleation. *Science* **2007**, *318*, 89–92.

(2) Sipilä, M.; Berndt, T.; Petäjä, T.; Brus, D.; Vanhanen, J.; Stratmann, F.; Patokoski, J.; Mauldin, R. L.; Hyvärinen, A.-P.; Lihavainen, H. et al. The Role of Sulfuric Acid in Atmospheric Nucleation. *Science* **2010**, *327*, 1243–1246.

(3) Kurtén, T.; Loukonen, V.; Vehkamäki, H.; Kulmala, M. Amines Are Likely to Enhance Neutral and Ion-Induced Sulfuric Acid-Water Nucleation in the Atmosphere More Effectively Than Ammonia. *Atmos. Chem. Phys.* **2008**, *8*, 4095–4103.

(4) Almeida, J.; Schobesberger, S.; Kürten, A.; Ortega, I. K.; Kupiainen-Määttä, O.; Praplan, A. P.; Adamov, A.; Amorim, A.; Bianchi, F.; Breitenlechner, M. et al. Molecular Understanding of Sulphuric Acid-Amine Particle Nucleation in the Atmosphere. *Nature* **2013**, *502*, 359–363.

(5) Zhang, R.; Suh, I.; Zhao, J.; Zhang, D.; Fortner, E. C.; Tie, X.; Molina, L. T.;

Molina, M. J. Atmospheric New Particle Formation Enhanced by Organic Acids. *Science* **2004**, *304*, 1487–1489.

(6) Zhang, R.; Khalizov, A.; Wang, L.; Hu, M.; Xu, W. Nucleation and Growth of Nanoparticles in the Atmosphere. *Chem. Rev.* **2012**, *112*, 1957–2011.

(7) Berndt, T.; Sipilä, M.; Stratmann, F.; Petäjä, T.; Vanhanen, J.; Mikkilä, J.; Patokoski, J.; Taipale, R.; Mauldin, R. L., III; Kulmala, M. Enhancement of Atmospheric $H_2SO_{4/}H_2O$ Nucleation: Organic Oxidation Products Versus Amines. *Atmos. Chem. Phys. Discuss.* **2013**, *13*, 16301–16335.

(8) Kupiainen-Määttä, O. A Monte Carlo Approach for Determining Cluster Evaporation Rates from Concentration Measurements. *Atmos. Chem. Phys.* **2016**, *16*, 14585–14598.

(9) Kürten, A. New Particle Formation from Sulfuric Acid and Ammonia: Nucleation and Growth Model Based on Thermodynamics Derived from CLOUD Measurements for a Wide Range of Conditions. *Atmos. Chem. Phys.* **2019**, *19*, 5033–5050.

(10) Kürten, A.; Jokinen, T.; Simon, M.; Sipilä, M.; Sarnela, N.; Junninen, H.; Adamov, A.; Almeida, J.; Amorim, A.; Bianchi, F. et al. Neutral Molecular Cluster Formation of Sulfuric Acid-Dimethylamine Observed in Real Time Under Atmospheric Conditions. *Proc. National Academy Sci. USA* **2014**, *111*, 14019–15024.

(11) Ortega, I. K.; Olenius, T.; Kupiainen-Määtä, O.; Loukonen, V.; Kurtén, T.; Vehkamäki, H. Electrical Charging Changes the Composition of Sulfuric Acid-Ammonia/Dimethylamine Clusters. *Atmos. Chem. Phys.* **2014**, *14*, 7995–8007.

(12) Zapadinsky, E.; Passananti, M.; Myllys, N.; Kurtén, T.; Vehkamäki, H. Modeling on Fragmentation of Clusters Inside a Mass Spectrometer. *J. Phys. Chem. A* **2019**, *123*, 611–624.

(13) Passananti, M.; Zapadinsky, E.; Zanca, T.; Kangasluoma, J.; Myllys, N.; Rissanen, M. P.; Kurtén, T.; Ehn, M.; Attoui, M.; Vehkamäki, H. How Well Can We Predict Cluster Fragmentation Inside a Mass Spectrometer. *Chem. Commun.* **2019**, *55*, 5946–5949.

(14) Bianchi, F.; Tröstl, J.; Junninen, H.; Frege, C.; Henne, S.; Hoyle, C. R.; Molteni, U.; Herrmann, E.; Adamov, A.; Bukowiecki, N. et al. New Particle Formation in the Free Troposphere: A Question of Chemistry and Timing. *Science* **2016**, *352*, 1109–1112.

(15) Halonen, R.; Zapadinsky, E.; Kurtén, T.; Vehkamäki, H.; Reischl, B. Rate Enhancement in Collisions of Sulfuric Acid Molecules Due to Long-Range Intermolecular Forces. *Atmos. Chem. Phys.* **2019**, *19*, 13355–13366.

(16) Carlsson, P. T. M.; Keunecke, C.; Krüger, B. C.; Maaß, M.-C.; Zeuch, T. Sulfur Dioxide Oxidation Induced Mechanistic Branching and Particle Formation During the Ozonolysis of β-Pinene and 2-Butene. *Phys. Chem. Chem. Phys.* **2012**, *14*, 15637–15640.

(17) Viisanen, Y.; Kulmala, M.; Laaksonen, A. Experiments on Gas-Liquid Nucleation of Sulfuric Acid and Water. *J. Chem. Phys.* **1997**, *107*, 920–926.

(18) Ball, S. M.; Hanson, D. R.; Eisele, F. L.; McMurry, P. H. Laboratory Studies of Particle Nucleation: Initial Results for H_2SO_4, H_2O and NH_3 Vapors. *J. Geophys. Res.* **1999**, *104*, 23709–23718.

(19) Carlsson, P. T. M.; Zeuch, T. Investigation of Nucleation Kinetics in H_2SO_4 Vapor Through Modeling of Gas Phase Kinetics Coupled With Particle Dynamics. *J. Chem. Phys.* **2018**, *148*, 104303.

(20) Wolf, J. L.; Richters, S.; Pecher, J.; Zeuch, T. Pressure Dependent Mechanistic Branching in the Formation Pathways of Secondary Organic Aerosol from Cyclic-Alkene Gas-Phase Ozonolysis. *Phys. Chem. Chem. Phys.* **2011**, *13*, 10952–10964.

(21) Carlsson, P. T. M.; Dege, J. E.; Keunecke, C.; Krüger, B. C.; Wolf, J. L.; Zeuch, T. Pressure Dependent Aerosol Formation from the Cyclohexene Gas-Phase Ozonolysis in the Presence and Absence of Sulfur Dioxide: a New Perspective on the Stabilisation of the Initial Clusters. *Phys. Chem. Chem. Phys.* **2012**, *14*, 11695–11705.

(22) Ahrens, J.; Carlsson, P. T. M.; Hertl, N.; Olzmann, M.; Pfeifle, M.; Wolf, J. L.; Zeuch, T. Infrared Detection of Criegee Intermediates Formed During the Ozonolysis of β-Pinene and Their Reactivity Towards Sulfur Dioxide. *Angew. Chem. Int. Ed.* **2014**, *53*, 715–719.

(23) Hoyermann, K.; Mauß, F.; Olzmann, M.; Welz, O.; Zeuch, T. Exploring the Chemical Kinetics of Partially Oxidized Intermediates by Combining Experiments, Theory, and Kinetic Modelling. *Phys. Chem. Chem. Phys.* **2017**, *19*, 18128–18146.

(24) Murphy, D. M.; Cziczo, D. J.; Hudson, P. K.; Schein, M. E.; Thomson, D. S. Particle Density Inferred from Simultaneous Optical and Aerodynamic Diameter Sorted by Composition. *J. Aerosol. Sci.* **2004**, *35*, 135–139.

(25) LOGEresearch, http://www.logesoft.com/loge-software/. **last accessed: May 2020**,

(26) Gelbard, F.; Seinfeld, J. H. Simulation of Multicomponent Aerosol Dynamics. *J. Colloid Interface Sci.* **1980**, *78*, 485–501.

(27) Wu, C.-Y.; Biswas, P. Study of Numerical Diffusion in a Discrete-Sectional Model and Its Application to Aerosol Dynamics Simulation. *Aerosol Sci. Tech.* **1998**, *29*, 359–378.

(28) Gelbard, F. Modeling Multicomponent Aerosol Particle Growth by Vapor Condensation. *Aerosol Sci. Tech.* **1990**, *12*, 399–412.

(29) Ortega, I. K.; Kupiainen, O.; Kurtén, T.; Olenius, T.; Wilkman, O.; McGrath, M. J.; Loukonen, V.; Vehkamäki, H. From Quantum Chemical Formation Free Energies to Evaporation Rates. *Atmos. Chem. Phys.* **2012**, *12*, 225–235.

(30) Henschel, H.; Kurtén, T.; Vehkamäki, H. Computational Study on the Effect of Hydration on New Particle Formation in the Sulfuric Acid/Ammonia and Sulfuric Acid/Dimethylamine Systems. *J. Phys. Chem. A* **2016**, *120*, 1886–1896.

(31) Riplinger, C.; Neese, F. An Efficient and Near Linear Scaling Pair Natural Orbital Based Local Coupled Cluster Method. *J. Chem. Phys.* **2013**, *138*, 034106.

(32) Riplinger, C.; Sandhoefer, B.; Hansen, A.; Neese, F. Natural Triple Excitations in Local Coupled Cluster Calculations with Pair Natural Orbitals. *J. Chem. Phys.* **2013**, *139*, 134101.

(33) Elm, J. An Atmospheric Cluster Database Consisting of Sulfuric Acid, Bases,Organics, and Water. *ACS Omega* **2019**, *4*, 10965–10974.

(34) Myllys, N.; Elm, J.; Halonen, R.; Kurtén, T.; Vehkamäki, H. Coupled Cluster Evaluation of the Stability of Atmospheric Acid-Base Clusters with up to 10 Molecules. *J. Phys. Chem. A* **2016**, *120*, 621–630.

(35) Elm, J.; Kristensen, K. Basis Set Convergence of the Binding Energies of Strongly Hydrogen-Bonded Atmospheric Clusters. *Phys. Chem. Chem. Phys.* **2017**, *19*, 1122–1133.

(36) Marti, J. J.; Jefferson, A.; Cai, X. P.; Richert, C.; McMurry, P. H.; Eisele, F. H_2SO_4 Vapor Pressure of Sulfuric Acid and Ammonium Sulfate Solutions. *J. Geophys. Res.* **1997**, *102*, 3725–3735.

(37) Kildgaard, J. V.; Mikkelsen, K. V.; Bilde, M.; Elm, J. Hydration of Atmospheric Molecular Clusters: A New Method for Systematic Configurational Sampling. *J. Phys. Chem. A* **2018**, *122*, 5026–5036.

(38) Kildgaard, J. V.; Mikkelsen, K. V.; Bilde, M.; Elm, J. Hydration of Atmospheric Molecular Clusters II: Organic Acid-Water Clusters. *J. Phys. Chem. A* **2018**, *122*, 8549–8556.

(39) Asmis, K. R.; Neumark, D. M. Vibrational Spectroscopy of Microhydrated Conjugate Base Anions. *Acc. Chem. Res.* **2012**, *45*, 43–52.

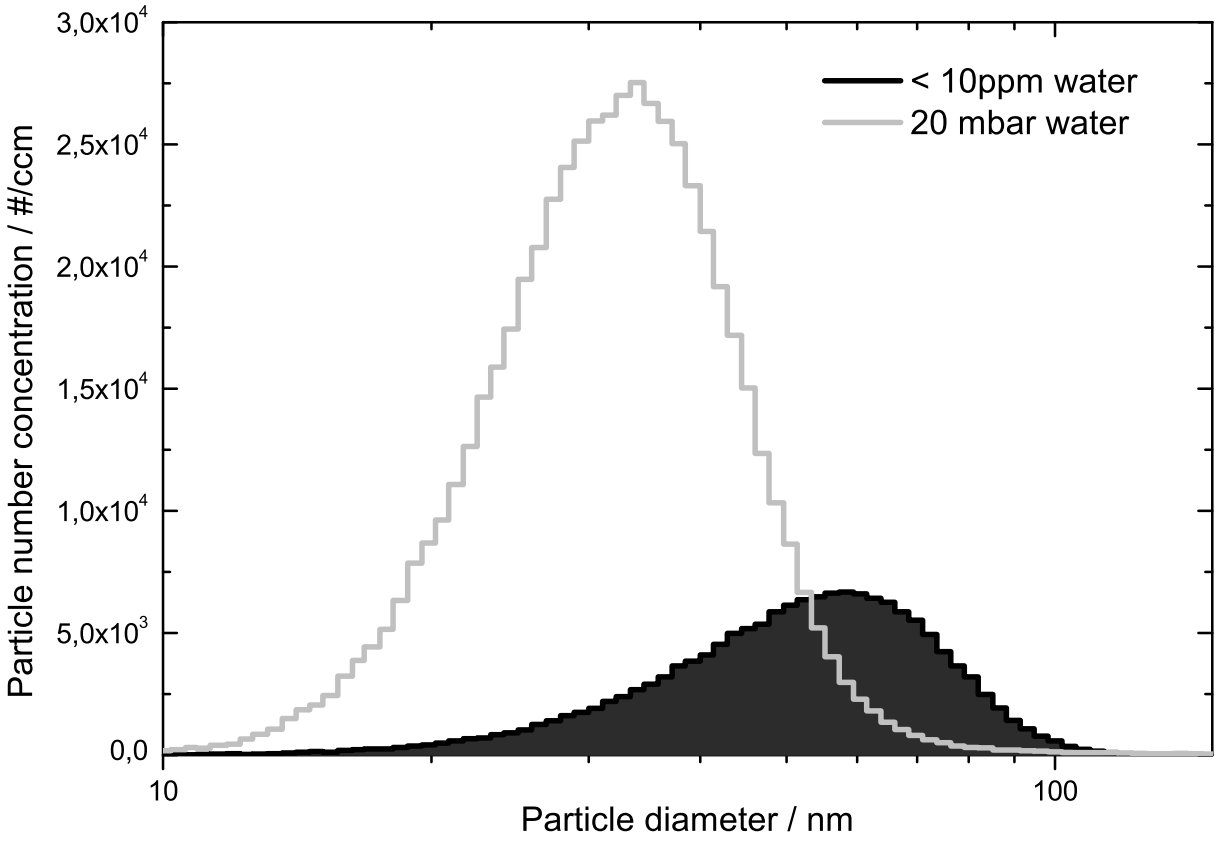

Figure 1: Comparison of two experimental size distributions (averaged from multiple individual distributions) at ∼10 ppm H_2O and 20 mbar H_2O partial pressures measured between 420 and 495 s after the initial expansion. Even the dry conditions are wet enough to efficiently form H_2SO_4 from SO_3.[16] The SO_2 concentrations were varied to account for the influence of the water content on H_2SO_4 yield via reactions of the water monomer and dimer with the Criegee intermediates. The dry case was performed with 10 ppb SO_2, the wet with 100 ppb. Fitting the individual size distributions with a lognormal function yielded an average particle mass concentration of $32.6 \pm 1.5\,\mu g\,m^{-3}$ for the dry and $25.3 \pm 3.1\,\mu g\,m^{-3}$ for the wet condition, using a density of $1.7\,g/cm^3$ for pure sulfuric acid particles.[24] This corresponds to simulated total H_2SO_4 yields of 7.8 ppb and 6.2 ppb, respectively.

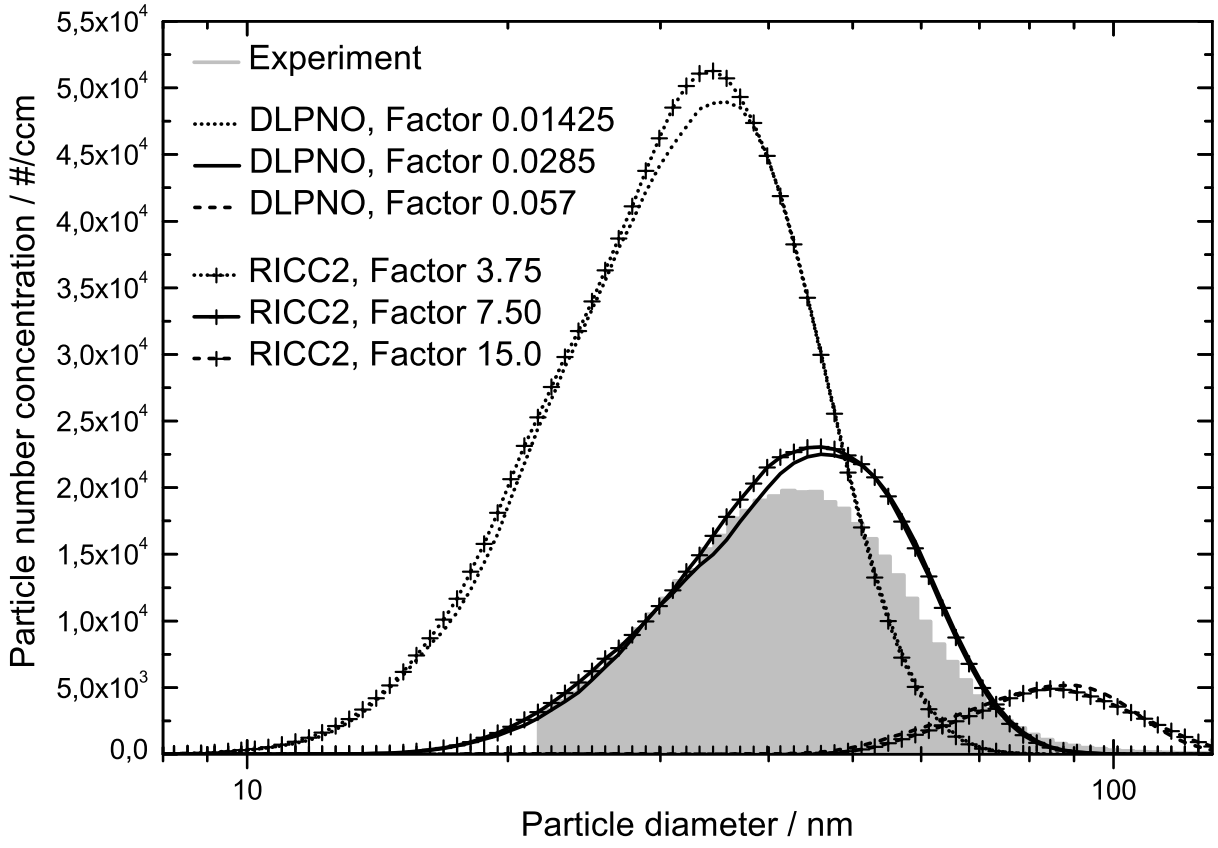

Figure 2: Comparison of an experimental size distribution (grey histogram, average over three individual scans) to those from simulation runs (simulated distribution was smoothed three times with the moving average method) with the decomposition rates from table 1 at 10 mbar H_2O and 100 ppb SO_2. The decomposition rates were multiplied by the value given in the legend to maximize agreement with the experiment (see also figure 4) and to show the clear difference induced by values only a factor of 2 different.

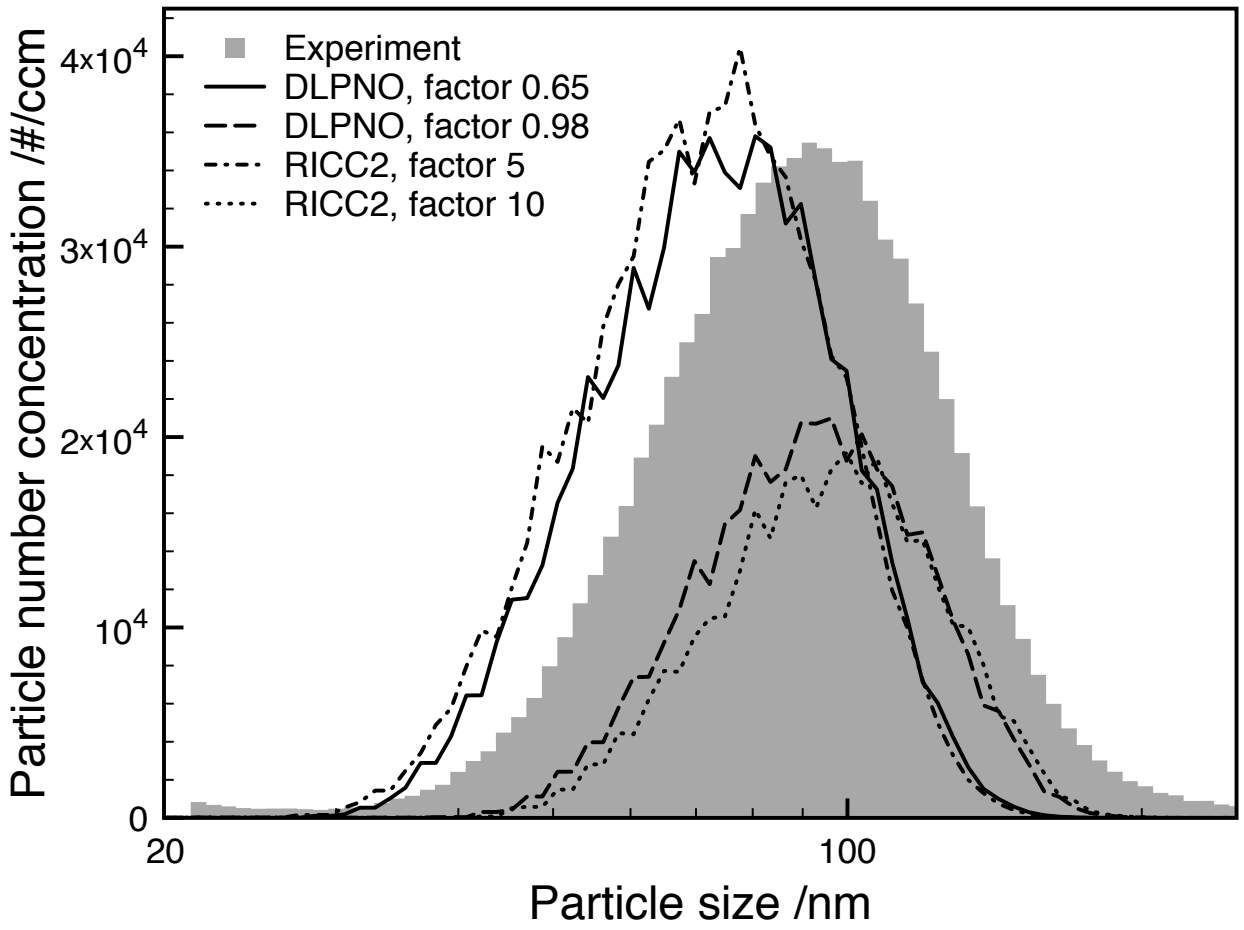

Figure 3: Comparison of an experimental size distribution (grey histogram) to those from simulation runs with varied decomposition rates for both theoretical methods, shown for 1 ppm initial SO_2 and dry conditions. Since a difference in mass is apparent due to either having the same total number but a lower mean size or alternatively the correct mean size but too few particles, this concentration of SO_2 lies in the regime with unknown further condensing species.

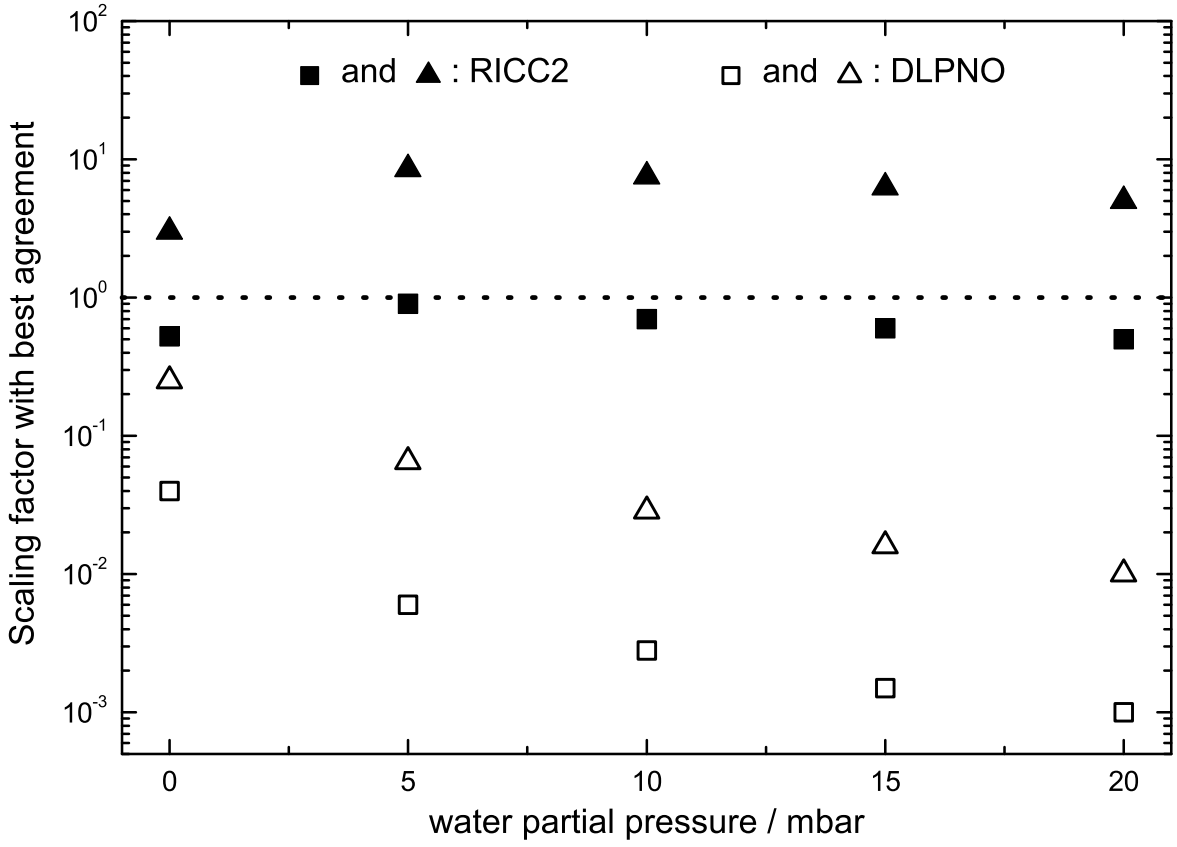

Figure 4: Comparison of the necessary scaling factors to bring simulations and experiments in agreement. Squares represent 10 ppb initial SO_2, triangles 100 ppb. The dotted line at unity facilitates the distinction between increasing and decreasing the decomposition rates.